

**Title: Giant Rashba-Splitting in 2D organic-inorganic halide perovskites
measured by transient spectroscopies**

Authors: Yaxin Zhai^{1, †}, S. Baniya^{1, †}, C. Zhang¹, J. Li^{2,3}, P. M. Haney², C.-X. Sheng^{1,4, *}, E. Ehrenfreund^{1,5}, Z.V. Vardeny^{1,*}

Affiliations:

¹Department of Physics & Astronomy, University of Utah, Salt Lake City, UT 84112, USA.

²Center for Nanoscale Science and Technology, National Institute of Standards and Technology, Gaithersburg, MD 20899, USA

³Maryland NanoCenter, University of Maryland, College Park, MD 20742, USA

⁴School of Electronic and Optical Engineering, Nanjing University of Science and Technology, Nanjing 210094, China

⁵Physics Department and Solid State Institute, Technion-Israel Institute of Technology, Haifa 32000, Israel

[†] These two authors contributed equally to the work.

*Correspondence to: val@physics.utah.edu; cxsheng@yahoo.com

Abstract: Two-dimensional (2D) layered hybrid organic-inorganic halide perovskite semiconductors form natural ‘multiple quantum wells’ that possess strong spin-orbit coupling due to the heavy elements in their building blocks. This may lead to ‘Rashba-splitting’ close to the extrema in the electron bands. We have employed a plethora of ultrafast transient, nonlinear optical spectroscopies, and theoretical calculations for studying the primary (excitons) and long-lived (free-carriers) photoexcitations in thin films of 2D perovskite, namely $(\text{C}_6\text{H}_5\text{C}_2\text{H}_4\text{NH}_3)_2\text{PbI}_4$. The density functional theory calculation shows the occurrence of Rashba-splitting in the plane perpendicular to the 2D barrier. From the electroabsorption spectrum and photoinduced absorption spectra from excitons and free-carriers we indeed obtain a giant Rashba-splitting in this compound, with energy splitting of (40 ± 5) meV and Rashba

parameter of $(1.6 \pm 0.1) \text{ eV}\cdot\text{\AA}$; which are among the highest Rashba-splitting size parameters reported so far. This finding shows that 2D hybrid perovskites have great promise for potential applications in spintronics.

One Sentence Summary: Optical spectroscopies and theoretical calculations provide compelling evidence of large Rashba splitting in 2D layered perovskite with Rashba parameter of $1.6 \text{ eV}\cdot\text{\AA}$ and energy of 40 meV.

Main Text:

The extrema points in the conduction and valence bands of semiconductors are of utmost importance in determining the optical, spin and transport properties of these materials. The electron dispersion relation, $E(k)$ near these extrema points are usually described by the effective-mass approximation, where the electrons and holes are treated as ‘free carriers’ having an effective mass, m^* , that leads to a spin-degenerate parabolic dispersion, $E(k)=\hbar^2k^2/2m^*$ (Fig. 1A). However, spin-orbit coupling (SOC) can split the spin-degenerate bands in non-centrosymmetric compounds, as first realized by Dresselhaus and Rashba (1, 2). More importantly the effect of SOC may be enhanced in reduced dimensions such as in two-dimensional (2D) semiconductors (3). In the presence of structural ‘inversion asymmetry’, the spin-degenerate parabolic band splits into two spin-polarized bands, where the electron (or/and hole) dispersion relation may be described by $E_{\pm}(k)=(\hbar^2k^2/2m^*)\pm\alpha_R|k|$, where α_R is the Rashba-splitting parameter. This formulation yields new extrema at a momentum offset (k_0) and energy splitting (E_R) that are related to each other via: $\alpha_R = 2E_R/k_0$ (4), see Fig. 1B. Importantly, the two Rashba-split branches have *opposite spins*, which can influence the photoexcitation’s optical and magnetic properties, a situation that may benefit spintronics since it enhances the spin-to-charge conversion efficiency (4, 5).

Large Rashba-splitting with α_R of few $\text{eV}\cdot\text{\AA}$ has been observed in only a handful of materials such as ultrathin metallic films (6), surfaces of topological insulators such as Bi_2Se_3 (7), and surfaces of the polar semiconductor BiTeI (8). We note that Rashba-splitting is very small in traditional III-V semiconductors. For example, the Rashba-splitting parameter α_R at the interface of $\text{InAlAs}/\text{InGaAs}$ was measured to be $\approx 0.07 \text{ eV}\cdot\text{\AA}$ with $E_R \approx 1 \text{ meV}$ (9). In contrast, here we

discovered a giant size Rashba-splitting in a 2D semiconducting layered hybrid organic-inorganic perovskite.

The 3D hybrid organic-inorganic perovskites (thereafter hybrid perovskites) such as methylammonium lead halogen (MAPbX_3 ; X is halogen) have recently attracted immense attention because of several promising optoelectronic device applications such as photovoltaic solar cells, light emitting diodes and lasers (10, 11). Importantly, these compounds possess strong SOC due to the heavy elements (Pb, X) that determine the electron bands near their extrema points, which may lead to large Rashba-splitting if the structure lacks inversion symmetry (12); this is in fact realized in some 2D and 3D hybrid perovskites (13). Interest in the hybrid perovskites for spintronics applications has only recently begun, with promising spin and magnetic field phenomena (14-15); therefore, solid evidence of Rashba-splitting existence in these compounds would further boost this interest.

Recently the 2D hybrid perovskites have come into focus (16, 17). These compounds self-assemble into alternating organic and inorganic layers that form natural ‘multiple-quantum wells’, with outstanding optoelectronic characteristics and stability at ambient conditions. Having strong SOC, high-charge mobility, and intrinsic quantum well structures with many interfaces and facile solution processability, the 2D hybrid perovskites may be promising candidates for room temperature spintronic applications (18). Our work shows that these materials may also exhibit giant Rashba-splitting, which could further enhance their appeal for this field.

We have employed a variety of transient and steady state linear and nonlinear optical spectroscopies as well as theoretical calculations for studying the optical characteristics of the primary (excitons) and long-lived (free-carriers) photoexcitations in 2D hybrid perovskite films (19). Fig. 1C shows schematically the 2D hybrid perovskite that we studied here, namely $(\text{C}_6\text{H}_5\text{C}_2\text{H}_4\text{NH}_3)_2\text{PbI}_4$ (PEPI), where the organic $(\text{C}_6\text{H}_5\text{C}_2\text{H}_4\text{NH}_3^+)$ and inorganic $[\text{PbI}_6]^{4-}$ octahedron layers form ‘multiple quantum wells’ with thickness of ≈ 1 nm (barrier) and ≈ 0.6 nm (well), respectively (20). A detailed description that includes energy gaps of the respective wells and barriers is given in Fig. S1 (19). The spectroscopies and model calculations employed in this work, as detailed in the Methods section (19), provide compelling evidence that the continuum band-edge above the exciton level (CB bottom and/or VB top) possesses surprising optical characteristic properties which result from a large Rashba-splitting energy, $E_R \approx 40$ meV. Our

work provides a general all-optical method for studying the Rashba-splitting effect in semiconductors.

The room-temperature photoluminescence (PL) and absorption spectra of the 2D hybrid perovskite PEPI film are dominated by an exciton band at ≈ 2.4 eV with large oscillator strength, consistent with a relatively large exciton binding energy, E_B of ≈ 0.2 eV (Fig. 1D) (21), followed by a slow increase in the absorption with an onset at ≈ 2.6 eV. At low temperatures ($T < 110$ K), however the absorption spectrum shows two step-like absorption edges in the spectral range of 2.45 eV to 2.65 eV (see Figs. 2A and S2 (19)). We thus used a modulation spectroscopy, namely the electroabsorption (EA) to separate these delicate absorption features from the broad spectral background. Recall that the EA spectrum in neat semiconductors having intermediately large E_B usually contains two different spectral features; a Stark shift of the exciton below the continuum, and a Frank-Keldysh (FK) type oscillatory feature at the continuum band-edge (22).

Figure 2B shows low temperature EA spectra of the PEPI obtained at various ac field strengths. Based on the EA dependence on the field strength (or V , the applied voltage), we indeed identify two distinctive EA spectral ranges. The EA scales with V^2 (Fig.S3) for $\hbar\omega < 2.55$ eV (23); but it saturates at large field for $\hbar\omega > 2.55$ eV (see Fig. 2D (inset)). The EA spectrum in the low energy spectral region (< 2.55 eV) shows a ‘first derivative-like’ feature consistent with an exciton Stark shift; having a zero-crossing at 2.38 eV that we assign as the 1s exciton energy, E_{1s} (Fig. 2F). We note that in this spectral region there is a second ‘derivative-like’ feature with ‘trending’ zero-crossing at ≈ 2.53 eV, in agreement with the lowest step-like feature in the absorption spectrum (Fig. 2A). We identify this EA feature as originating from the 2s exciton in PEPI (24), as shown in Fig. 2F (13, 25).

In contrast, the large oscillatory-like EA feature at $\hbar\omega > 2.55$ eV having multiple zero-crossings is due to FK oscillation above the direct band-edge (22, 26). Importantly, the oscillation energy period, δE shows ‘field-broadening’ that scales with $V^{2/3}$ (see Figs. 2C, 2D and 2E). This broadening and the EA saturation at large V are typical characteristic properties of the FK oscillation in the EA spectrum close to the band edge (Inter-band (IB) transition in Fig. 2B), where the peak at energy below the first zero-crossing determines the energy gap value. We thus locate the band-edge of the PEPI film at 2.57 eV (Fig. 2B). From $E(\text{IB})$, E_{1s} and E_{2s} we can now obtain the 1s and 2s exciton binding energies: $E_B(1s) = (190 \pm 4)$ meV and $E_B(2s) = (45 \pm 8)$ meV, respectively. The uncertainty originates mainly from the optical resolution of our

spectrometer (2 nm entrance slit size) and the film inhomogeneity; all uncertainties are reported as one standard deviation.

To further investigate the excited state properties of PEPI close to the continuum band minima, we studied the primary photoexcitations using the picosecond (ps) transient photomodulation (PM) with 250 fs time resolution in a broad spectral range of 0.23 eV to 2.8 eV, excited at 3.1 eV (see Method in (19)). The PM spectrum contains photoinduced absorption (PA) bands with $\Delta T < 0$ due to excited state absorption; and photoinduced bleaching (PB) with $\Delta T > 0$ caused by pump-induced bleaching of the ground state absorption. At $t = 0$ ps the PM spectrum contains two dominant spectral features (Fig. 3A); a PA band in the mid-IR spectral range, denoted PA₁ at ≈ 0.35 eV, and a PM feature in the visible spectral range centered at the PEPI exciton absorption (≈ 2.4 eV) having both PA and PB components; as well as a weak PA band at ≈ 1 eV denoted PA₂. We note the occurrence of ‘zero-sum’ when adding the PA and PB bands of the entire PM spectrum, indicating that there are no other important photoinduced features in the spectrum. Also the PA and PM bands share similar decay dynamics (Fig. 3B), which supports the notion that they originate from a *single* primary photoexcitation species. We note that the PB dynamics contains a much slower component that is represented by a constant in the decay fitting (Fig. 3B), indicating that some long-lived photoexcitation survive the fast exciton recombination; these may be photocarriers as discussed below.

The PM band in the visible range can be fit by linear combination of PB of the absorption spectrum, and the absorption first and second derivatives, as shown in Fig. S4 (19). It therefore can be explained by a combination of ‘band-filling’ due to the primary photoexcitation (27), photoinduced symmetry breaking process such as spatially inhomogeneous strain or photoinduced electric field (18, 28), and transient broadening (29). From the exciton PB in the PM spectrum and strong PL emission from PEPI (Fig. 1D) we conclude that the primary photoexcitations in this 2D perovskite are *excitons*, mainly 1s excitons. We can therefore study the electron bands simply from the exciton transition into the adjacent continuum band(s), as schematically depicted in Fig. 3C.

The PA₁ band from the excitons into the continuum band peaks at 350 (± 1) meV (the uncertainty comes from the 150 fs pulse duration), which cannot be ascribed to the vertical transition from the 1s exciton into the lowest continuum band, since from our EA studies, a transition into the lowest continuum band should appear at 190 meV. We therefore assign PA₁ to

an optical transition from the 1s exciton to a second, upper electron continuum branch which is split from the lower band by Rashba spin-orbit coupling, as shown schematically in Fig. 3C. We have looked for a second PA band at ≈ 0.2 eV (i.e. into the lower continuum band), but could not find any hint of it down to 0.23 eV (see Fig. 3A inset). Our finding suggests that a direct optical transition from the exciton into the lower Rashba-split branch is either forbidden or much weaker compared to that in traditional semiconductors such as GaAs (30). To rationalize this result, we note that the transition from a 1s exciton to a band minimum of free electron-hole pairs is proportional to the electrical dipole moment matrix element between a conduction (valence) band state and itself. This is because the initial exciton includes a Bloch state of the conduction band minimum, and the final electron-hole pair includes this same Bloch state. This matrix element is nothing more than the momentum expectation value of the Bloch state, which vanishes at the band minimum. In previous analysis of the exciton-CB transition in GaAs (30), the authors replaced the free carrier wave function by a p -state of an unbound electron-hole pair wave function, enabling the dipole transition exciton \rightarrow continuum band. In our 2D perovskite film, disorder from point defects and grain boundaries may destroy the coherence of the unbound electron-hole pair, so that optical transitions rely solely on the properties of the Bloch wave functions. Fig. 4D shows the density functional theory calculation of various electrical dipole transition matrix elements, which verifies that only transitions into the upper Rashba-split conduction band are allowed (19).

We can now obtain the Rashba-splitting energy, E_R from the PA_1 band at 350 meV, since PA_1 should be pushed to higher energies by an energy, $\Delta E=4E_R$; namely $E(PA_1)=E_B+4E_R$ (Fig. 3C). Using this relation, E_B (=190 meV from the EA spectrum) and $E(PA_1)=350$ meV (from the transient PA spectrum), we determine $E_R=(40\pm 5)$ meV in 2D PEPI. We note that PA_1 spectrum is asymmetric; this may be due to the transition from the exciton discrete level to the continuum band, where the exciton wave function is spread in k -space by a ' k -localization length' Δk , as determined by its 'localization length', l in real space, and $\Delta k \approx 1/l$ (18) (see discussion in (19)). In the inset of Fig. 3A, the solid line through the PA_1 data points is a fit using the optical transition model for a 2D semiconductor described in Eq. (S4) (19), from which we obtain the exciton localization length $l \approx 10$ nm (19). This relatively large l -value indicates that the exciton is quite delocalized in the quantum well in a direction perpendicular to the barriers; but localized in k -space. Also the weak PA_2 band at ≈ 1 eV may be readily explained as the optical transition from

the exciton level at ≈ 2.4 eV into higher lying bands at ≈ 3.3 eV, which can be clearly seen in the absorption spectrum (Fig. S2); similar as in the transient PM spectra of excitons in nanotubes and in $\text{CH}_3\text{NH}_3\text{PbI}_3$ (31).

Furthermore, we expect that the presence of Rashba-splitting would affect the process that leads to free carrier absorption (FCA). To investigate this assumption, we studied the properties of long-lived photoexcitations in PEPI using the technique of steady state PM (see Methods in (19)). The long-lived photoexcitations should be free-carriers since the excitons have a sufficiently long time to ionize into free electrons and holes that can contribute to photocarriers, especially at grain boundaries. This has been verified in PV cells based on 2D perovskites that have shown power conversion efficiency larger than 10 % (16). In this case the PM spectrum would be due to photogenerated FCA.

To verify that we can indeed measure photoinduced FCA by our PM technique we measured, as a ‘control experiment’ the steady-state PM spectrum in crystalline Si at 45 K, as seen in Fig. 5A. We could readily fit this PA spectrum by a Drude-type FCA response in which the PA spectrum varies as ω^{-2} (32); this validates our approach. In contrast, the steady state PA spectrum (PA_{FCA}) in PEPI film shows a sharp dip at low photon energy forming a peak at $\hbar\omega \approx 0.15$ eV. We consider this surprising FCA(ω) response a ‘smoking-gun’ verification of the Rashba-splitting that exists in the PEPI continuum band. Since optical transitions within the same branch can only be Drude-like that is allowed because of the mixture of s and p states in the CB (19), we ascribe this PA band to FCA with an onset at the vertical transition from the bottom of one branch of the CB into the other branch, as shown schematically in Fig. 5B. This transition is allowed since it involves states of non-zero k value for the upper and lower spin-split branches of the CB and therefore mixture of s and p states (see details in (19)).

The obtained FCA peak at 0.15 eV is in excellent agreement with the optical transition of the excitons (PA_1) measured by the ps transient PM (Fig. 3A), since both transitions contain an ‘add-on’ energy, $\Delta E = 4E_R$ (see Figs. 3D and 5B). From the FCA peak at 0.15 eV we obtain Rashba-splitting energy, $E_R \approx (38 \pm 3)$ meV. Another source of uncertainty in this measurement is the unknown value of the quasi-Fermi level at the CB bottom, which may well be of order 2-3 meV at low temperature. We therefore conclude that the FCA results are in excellent agreement with $E_R = 40 (\pm 5)$ meV determined from the transient ps spectroscopy.

From the obtained E_R value, we can readily estimate the offset, k_0 in the momentum space using a parabolic dispersion relation with an electron effective mass obtained using density function theory $m^* = 0.25 m_0$ (where m_0 is the bare electron mass); we thus obtained $k_0 = (0.051 \pm 0.004) \text{ \AA}^{-1}$. Consequently we estimate the Rashba splitting parameter $\alpha_R = (1.6 \pm 0.1) \text{ eV} \cdot \text{ \AA}$. These values are comparable to the recently measured Rashba parameters in MAPbBr₃ using the surface-sensitive angle-resolved photo-electron spectroscopy (ARPES; (34)).

To help understand the origin of the Rashba spin-orbit splitting of the conduction band, we carry out first-principles density functional theory (DFT) calculations using local density approximation (LDA) in the form of ultrasoft pseudopotentials as implemented in QUANTUM-ESPRESSO (19). Fig. 4A shows the geometry of the relaxed structure. We find that the inversion symmetry is broken due to the Pb atom displacement from the octahedra center. The displacement is in the 2D plane, roughly in the direction of $\mathbf{a} + \mathbf{b}$, where \mathbf{a} , \mathbf{b} are the in-plane lattice vectors. This leads to the Rashba band splitting for states with crystal momentum oriented perpendicular to symmetry breaking direction, as shown in Fig. 4C. The dashed red and blue lines in Fig. 4D show the optical transition matrix elements within the lowest conduction band, which, as discussed above, vanish at the minimum of the energy dispersion. The solid green line denotes the inter-band matrix element, which does not vanish at this point, indicating that the optical transition is allowed. An effective tight-binding model given in the S.I. (19) shows that the source of this optical transition is sp hybridization present in the conduction band eigenstates at the band minimum. From our model calculation we obtain band splitting $E_R = 160 \text{ meV}$, which is larger than the experimentally determined splitting. We attribute this discrepancy to approximations used in LDA. For more quantitatively accurate description of the electronic structure, a calculation at the level of quasiparticle GW is likely required.

In conclusion, strong spin orbit coupling in the 2D perovskite PEPI causes Rashba-splitting in the continuum band, where the spin-degenerate parabolic band splits into two branches with opposite spin-aligned electronic states. This causes both the optical transitions of excitons into the continuum band, and free carrier absorption within the continuum band to acquire an ‘add-on’ energy term of $4E_R$. From the peak of the exciton transition measured by ps transient PM, and the FCA measured by steady state PM we have determined the Rashba-splitting energy, $E_R = (40 \pm 5) \text{ meV}$ in PEPI 2D hybrid perovskite, which is among the highest values reported so

far. Our work provides a comprehensive, all optical method for studying the Rashba-splitting effect in semiconductors.

References and Notes:

1. G. Dresselhaus, A. Kip, C. Kittel, *Phys. Rev.* **95**, 568-569 (1954)
2. E.I. Rashba, *Sov. Phys. Solid State* **2**, 1109-1122 (1960).
3. Y.A. Bychkov & E.I. Rashba, *JETP Lett.* **39**, 78-81 (1984).
4. A. Manchon, *et al.*, *Nature Materials*, **14**, 871-882 (2015)
5. E. Lesne, *et al.*, *Nature Materials* **15**, 1261(2016)
6. E. Frantzeskaikis *et al.*, *Phys. Rev. Lett.* **101**, 196805 (2008)
7. P.D.C. King *et al.*, *Phys. Rev. Lett.* **107**, 096802(2011),
8. K. Ishizaka *et al.*, *Nat. Materials* **10**, 521-526(2011)
9. J. Nitta *et al.*, *Phys. Rev. Lett.* **78**, 1335-1338 (1997),
10. S.D. Stranks & H.J. Snaith, *Nat. Nanotechnology* **10**, 391-402(2015)
11. N.G. Park *et al.*, *Nat. Energy* **1**, 16152(2016)
12. Z.G. Yu, *Sci. Reports*, **6**, 28576 (2016)
13. M. Kepenekian, *et al.*, *ACS Nano* **9**, 11557-11567 (2015)
14. C. Zhang, *et al.* *Nat. Phys.* **11**, 427-434(2015).
15. Y.-C. Hsiao *et al.*, *Adv. Mater.* **27**, 2899–2906 (2015)
16. H. Tsai *et al.*, *Nature* **536**, 312–316 (2016).
17. D.H. Cao *et al.*, *J. Am. Chem. Soc.* **137**, 7843–7850 (2015).
18. D. Giovanni *et al.*, *Science Advance* **2**, e1600477 (2016)
19. Materials and methods are available as supplementary materials.
20. J. Fujisawa, T. Ishihara, *Phys. Rev. B*, **70**, 205330 (2004)
21. X. Hong *et al.*, *Phys. Rev. B*, **45**, 6961-6964 (1992)
22. L. Sebastian & G. Weiser, *Phys. Rev. Lett.* **46**, 1156-1159 (1981)
23. M. E. Ziffer, *et al.*, *ACS Photonics*, **3**, 1060-1068 (2016)
24. O. Yaffe, *et al.*, *Phys. Rev. B* **92**, 045414 (2015)
25. Y. Yacoby, *Phys. Rev.* **140**, A263-A270 (1965)
26. D.E. Aspnes, *Phys. Rev.* **153**, 972-982 (1967)
27. C.-X. Sheng, *et al.*, *Phys. Rev. Lett.* **114**, 116601 (2015)
28. G.S. Kanner, *et al.*, *Phys. Rev. Lett.* **74**, 1685-1688 (1995)
29. K. Abdel-Baki, *et al.*, *J. Appl. Phys.* **119**, 064301 (2016)
30. R.A. Kaindl, *et al.*, *Nature* **423**, 734-736 (2003)
31. C.-X. Sheng, *et al.*, *Syn. Metals* **216**, 31-39 (2016)
32. M. Fox, *Optical Properties of Solids*, (Oxford University Press, 2001)
33. Z. Guo, *et al.*, *ACS Nano* **10**, 9992 (2016)
34. D. Niesner *et al.*, *Phys. Rev. Lett.* **117**, 126401 (2016)

Acknowledgments: We are grateful to Dr. Dali Sun (NCSU) for helpful discussions. The work at the University of Utah was supported by the Department of Energy Office of Science, grant DE-SC0014579. The film growth facility, C.Z. and S.B. were supported by the National Science Foundation-Material Science & Engineering Center (NSF-MRSEC) program at the University of Utah, grant DMR 1121252. E.E. acknowledges support from the Israel Science Foundation, grant No 598/14.

The authors declare that there is no conflict of interests associated with this work. The project was planned by Z.V.V. Films were grown and characterized by C.Z. All the measurements were conducted by Y.Z., S.B., and C.X.S. The data analysis was performed by Z.V.V., C.X.S. and E.E. The calculations were done by P.M.H. and J.L. The manuscript was prepared by Z.V.V, C.X.S and P.M.H. and discussed with all other co-authors.

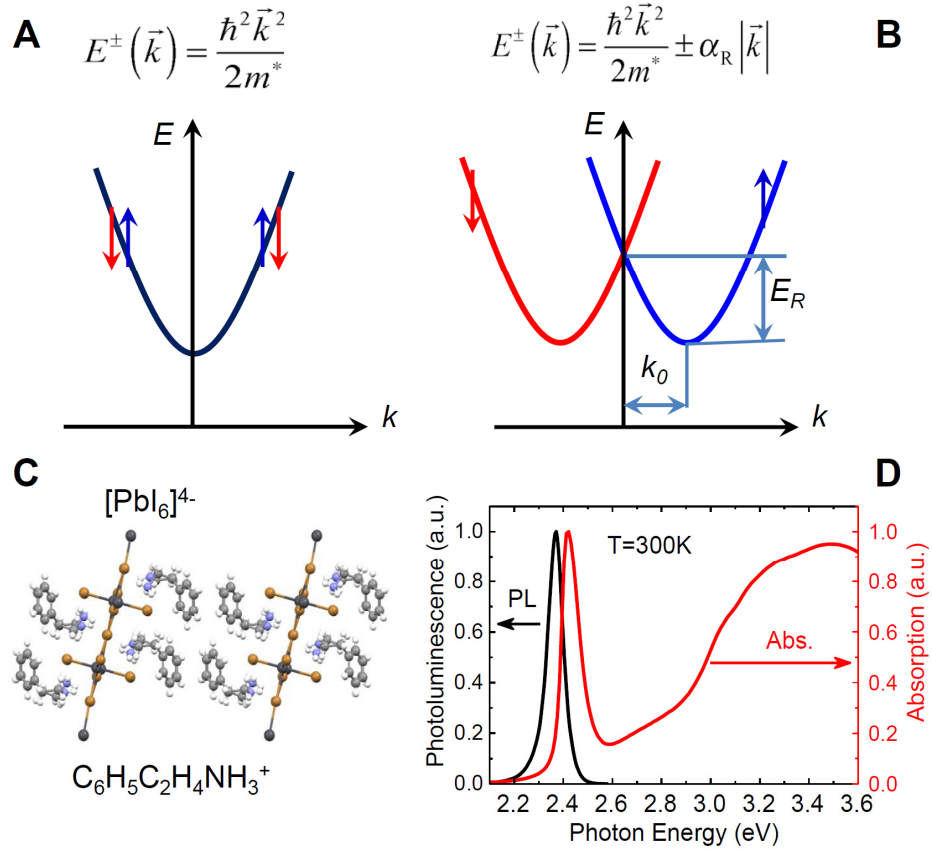


Fig.1.| Introduction to Rashba-splitting and the 2D layered hybrid perovskite $(\text{C}_6\text{H}_5\text{C}_2\text{H}_4\text{NH}_3)_2\text{PbI}_4$ (PEPI). **A:** Schematic electron dispersion relation of a regular conduction band (CB) that shows a doubly spin-degenerate parabolic band having a single minimum at $k=0$. **B:** Same as in A but subjected to Rashba-splitting; two parabolic branches having opposite spin sense are formed. The Rashba energy (E_R) and momentum offset (k_0) are denoted. **C:** The structure of PEPI having alternating organic ($\text{C}_6\text{H}_5\text{C}_2\text{H}_4\text{NH}_3^+$) and inorganic ($[\text{PbI}_6]^{4-}$) layers that form ‘multiple quantum wells’. **D:** The absorption (Abs) and photoluminescence (PL) spectra of PEPI film at room temperature (RT).

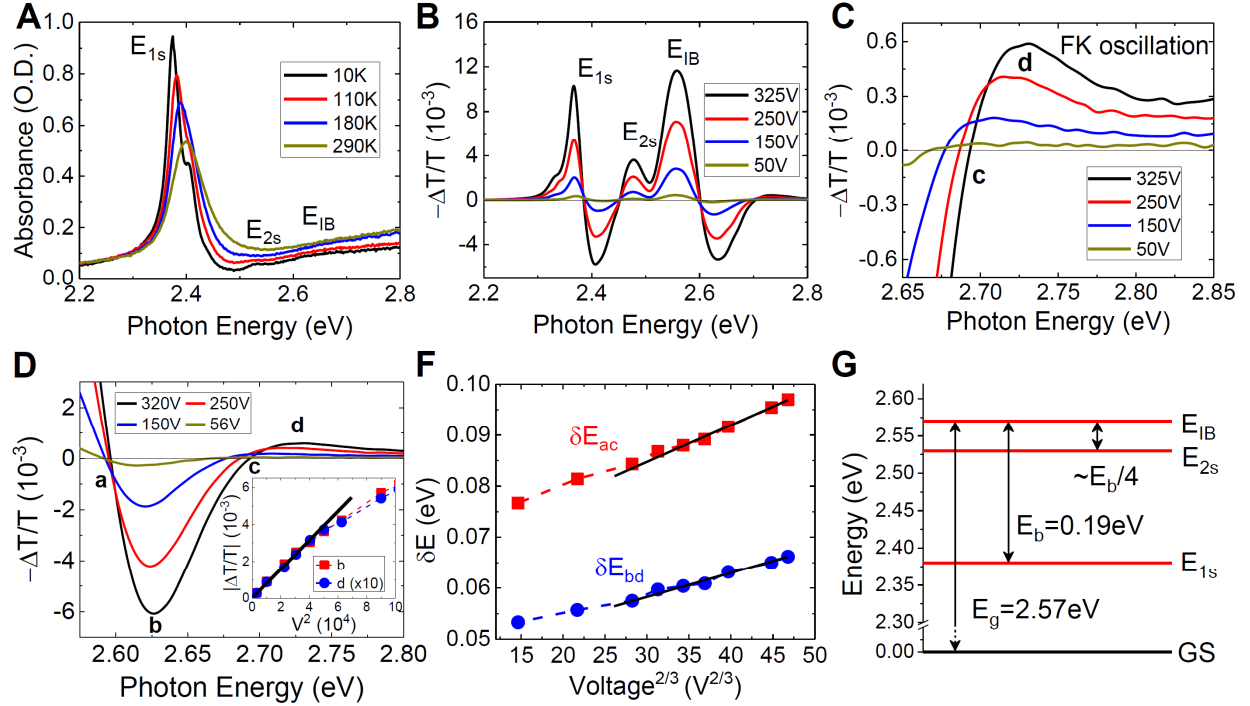


Fig. 2. | Absorption and electroabsorption (EA) spectra of PEPI film. **A:** absorption spectra of PEPI film at various temperatures. The 1s and 2s exciton (E_{1s} and E_{2s} , respectively) and an interband transition (IB) are assigned. **B:** EA spectra of PEPI measured at 45K at various applied electric fields (\sim the applied voltage, V). Various EA spectral features are assigned, where FK stands for the Franz-Keldysh oscillation. **C:** EA spectra close to the zero-crossing energy measured at various field strengths; broadening of the FK oscillation is clearly seen. “d” symbolizes the high-energy FK oscillation that blue-shifts with increasing field. **D:** Field broadening of the EA features related to the FK oscillation; ‘a’, ‘c’, ‘b’ and ‘d’ are assigned as zero-crossing energies and peak positions, respectively. The inset shows the peak values of EA vs V^2 of bands ‘b’ and ‘d’, which saturate at large V . **E:** The energy difference δE_{ac} and δE_{bc} plotted vs $V^{2/3}$. **F:** Energy levels of the excitons (E_{1s} , E_{2s}) and interband transition (E_{IB}) are assigned respect to the ground state (GS).

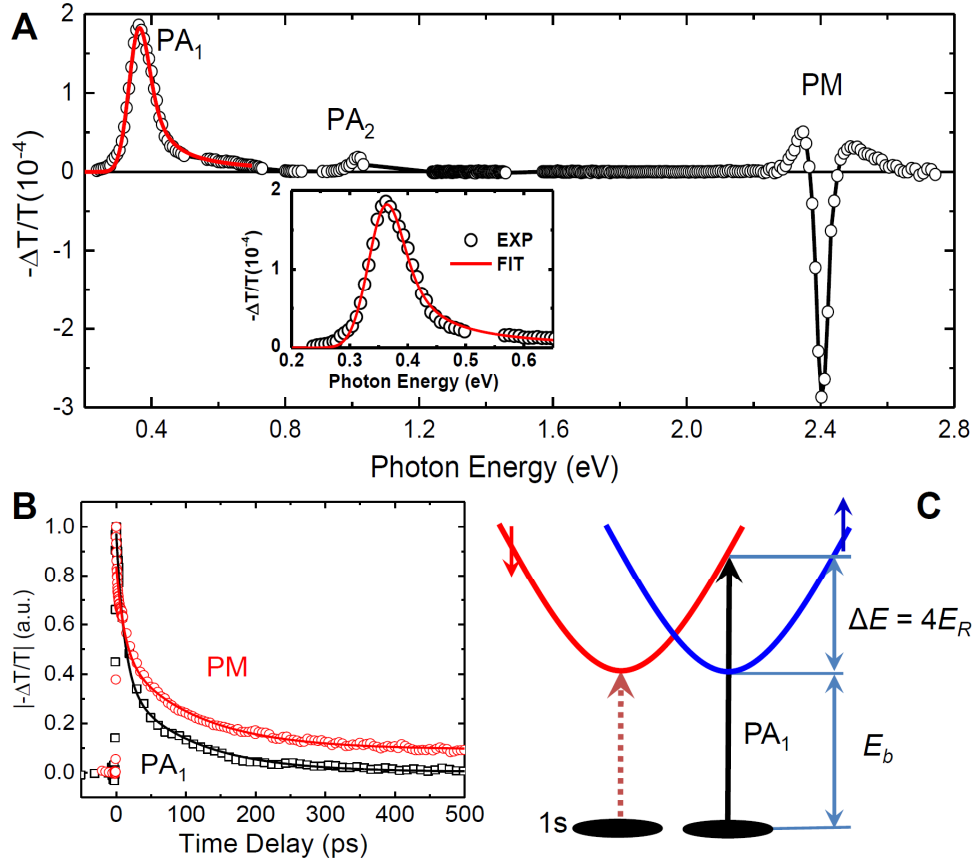


Fig. 3. Ultrafast photomodulation spectroscopy of PEPI film excited at 3.1 eV. **A:** PM spectrum at $t = 0$ ps; PA₁, PA₂, and PM are assigned. The solid line through the data points of PA₁ shown in the inset is a fit using a theoretical model for the exciton transition into the continuum (see text and (19)). **B:** Decay dynamics of the PM band at 2.4 eV and PA₁ at 0.36 eV up to 500 ps. The lines through the data points are fits using double exponential decay ($\sim A_1 e^{-t/t_1} + A_2 e^{-t/t_2} + C$); where $t_1 = 11.9$ ps, 11.8 ps; $t_2 = 103$ ps, 108 ps; and $C = 0.003$ and 0.094, for PA₁ and PM bands, respectively; **C:** Schematic energy diagram with Rashba-splitting that explains the PA₁ transition. The Rashba energy (E_R) may be obtained from the 1/4 of energy difference (ΔE) between PA₁ transition and the 1s exciton binding energy (E_b).

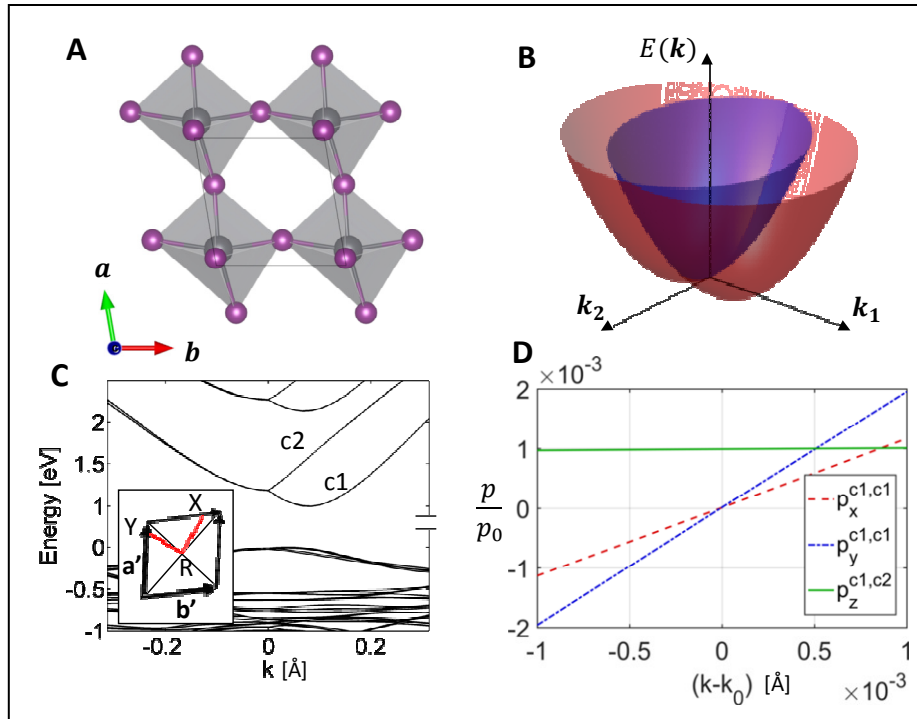


Fig. 4| A: One layer of the Pb-I octahedra that describes the relaxed structure of the PEPI used in the DFT calculations. The Pb atom (grayish sphere) is displaced from the octahedra center, along the $\mathbf{a}+\mathbf{b}$ direction, which breaks of the inversion symmetry resulting in Rashba-splitting caused by spin-orbit coupling. The unit cell vectors \mathbf{a} and \mathbf{b} lie in the x-y plane with an angle 99.7° between them. **B:** Schematic of the CB energy dispersion near the R point in the BZ, where $\mathbf{k}_{1(2)}$ is directed along the $\mathbf{a}-(+)\mathbf{b}$ direction. **C:** Electronic band structure near the R point, which shows the Rashba-splitting along a direction perpendicular to the symmetry breaking direction; c1 and c2 label the lower and upper Rashba bands, respectively. **D:** The DFT-calculated momentum matrix elements vs. k near the band minimum (at $k_0 = 0.07 \text{ \AA}^{-1}$) away from the R point along the (1, -1) direction). Red and blue lines correspond to x and y component of the momentum matrix element between lowest conduction band c1 and itself, showing the vanishing transition between the exciton and lowest Rashba-split CB at $k=k_0$. The green curve is the z component of the momentum matrix element between the Rashba-split bands c1 and c2, which is nonzero for all k . The y-axis is dimensionless, with the computed momentum, as the computed momentum p is presented in terms of its value in Rydberg units: $p_0 = 1.99 \times 10^{-24} \text{ kg/(m}\cdot\text{s)}$.

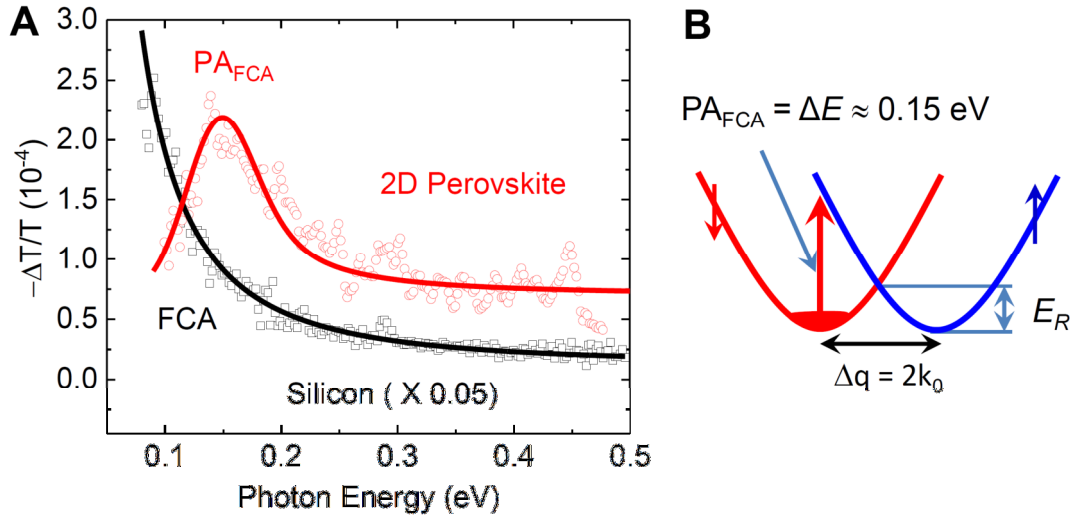


Fig. 5. | Steady state photomodulation spectroscopy of PEPI film excited at 2.8 eV. A: PM spectrum of PEPI film compared to that of a silicon wafer measured at modulation frequency of 350 Hz, and temperature of 45K. The PA bands, PA_{FCA} for PEPI and FCA (free carrier absorption) for Si are assigned. The solid lines through the data points are fits using the Drude model ($PA \sim \omega^{-2}$) for the Si wafer and Eq. S4 for the PEPI (19). **B:** Schematic electron energy bands with Rashba-splitting that explains the FCA in PEPI. The Rashba energy (E_R) and momentum offset ($k_0 = \Delta q/2$) are assigned.

Supplementary Materials:

Materials and Methods

Supplementary Text

Figures S1-S4

References (S1-S6)

Supplementary Materials for

Giant Rashba Splitting in two-dimensional layered halide hybrid perovskite semiconductors measured by optical spectroscopies

Yaxin Zhai^{1, †}, S. Baniya^{1, †}, C. Zhang¹, Junwen Li^{2,3}, P. M. Haney², C.-X. Sheng^{1, 4, *}, E. Ehrenfreund⁵, Z.V. Vardeny^{1,*}

¹Department of Physics & Astronomy, University of Utah, Salt lake City, UT 84112, USA.

² Center for Nanoscale Science and Technology, National Institute of Standards and Technology, Gaithersburg, MD 20899, USA

³ Maryland NanoCenter, University of Maryland, College Park, MD 20742, USA⁴School of Electronic and Optical Engineering, Nanjing University of Science and Technology, Nanjing 210094, China

⁵Physics Department and Solid State Institute, Technion-Israel Institute of Technology, Haifa 32000, Israel

*Correspondence to: val@physics.utah.edu; cxsheng@yahoo.com

This PDF file includes:

Materials and Methods
Supplementary Text
Figs. S1 to S4
References S1 to S7

Materials and Methods

Sample preparation:

The 2D hybrid perovskite films were fabricated in a nitrogen-filled glove box with oxygen and moisture levels $< 1 \mu\text{g/g}$. We mixed R-NH₃I (where R is C₆H₅C₂H₄) and PbI₂ in a 2:1 mole ratio in N,N-dimethylformamide to form solutions with a concentration of 0.5 mol/ml. The solutions were spin-coated on an Oxygen plasma pretreated sapphire or KBr substrates at 420 rad/sec and 90 s, to form 100 nm thick films; the obtained films were subsequently annealed at 100°C for 30 min. The purchased chemicals were used without further purification. All samples were prepared in a nitrogen-filled glove box with oxygen and moisture levels $< 1 \mu\text{g/g}$. From the high transmission through the film and the observation of numerous diffraction orders (see Fig. S2) we conclude that our spectroscopies are performed on high quality films.

Optical Spectroscopies

The main technique that we used in the present study for measuring the primary photoexcitation in the 2D hybrid perovskites is the transient photomodulation (PM) spectroscopy using the pump-probe correlation method. In this technique, the pump pulse excites the sample and the mechanically delayed probe pulse measures the pump-induced changes, $\Delta T(t)$ in the sample transmission, T . The PM spectrum contains photoinduced absorption (PA) bands with $\Delta T < 0$ due to excited state absorption; and photoinduced bleaching (PB) with $\Delta T > 0$ caused by pump-induced bleaching of the ground state absorption. We used two laser systems based on Ti:Sapphire oscillator. These are: a low power (energy/pulse ≈ 0.1 nJ) high repetition rate (≈ 80 MHz) laser for the mid-IR spectral range; and a high power (energy/pulse ≈ 10 μJ) low repetition rate (≈ 1 kHz) laser for the near-IR/visible spectral range. The pump excitation for both laser systems was set at $\hbar\omega = 3.1$ eV. For the low intensity measurements in the mid-IR spectral range we used an optical parametric oscillator (Opal, Spectral-Physics) that generates $\hbar\omega(\text{probe})$ from 0.25 eV to 1.05 eV. Whereas for the high intensity measurements, white light super-continuum was generated for $\hbar\omega(\text{probe})$ ranging from 1.15 eV to 2.7 eV. The transient PM spectra from the two laser systems were normalized to each other using the fundamental (1.55 eV) probe from the low power laser system. For the PM spectrum in the visible spectral range we used a Si photodiode, whereas for the mid-IR spectral range we used an InSb photodiode that was cooled to 80K to minimize the dark electrical noise.

For the EA measurements, we used a 2D perovskite film fabricated on a substrate with patterned metallic electrodes. The EA substrate consisted of two interdigitated sets of a few hundred of 10 μm wide gold electrodes, which were patterned on a sapphire substrate. The device was placed in a cryostat for low temperature measurements. By applying a potential, V to the electrodes a typical electric field, $F \approx 10^5$ Volt/cm was generated with $V = 300$ Volts and $f = 1$ kHz parallel to the film. For probing the EA spectrum, we used an incandescent light source from a Xe lamp, which was dispersed through a monochromator, focused on the sample, and detected by a UV-enhanced silicon photodiode. We measured the changes, ΔT in the transmission spectrum, T using a lock-in amplifier, set to twice the frequency ($2f$) of the applied field, and verified that no EA signal was observed at f or $3f$. ΔT and T spectra were measured separately using a Si photodiode and the EA spectrum was obtained from the ratio $\Delta T/T$.

For the the CW PM measurements, the excitation pump was provided by a diode laser with $\hbar\omega = 2.8$ eV, and the probe beam was provided by an incandescent tungsten/halogen lamp (for the visible-near infrared) or a globar light source (for mid-infrared). The sample films grown on KBr

substrates were put in a cryostat under vacuum. The sample temperature was varied from 50 K to 300 K. The pump and probe beams were overlapped on the sample films, and the transmitted probe beam was filtered through a monochromator and detected by a Si, InGaAs or HgCdTe detector for different probe spectral ranges. The transmission, T and change of the transmitted probe beam (ΔT), which was caused by the modulated pump beam, was detected by a lock-in amplifier. The PA spectrum was then calculated from $\Delta T/T$.

Supplementary Text

Fitting the PA₁ band at t=0 ps shown in Fig. 3A

In the momentum (k) space of a quantum well the energy dependent absorption coefficient $\alpha(E)$ of electron from the exciton state into the continuum can be expressed [S3] as,

$$\alpha(E) \propto \frac{1}{E} \int d^2k |M(k)|^2 [f(E_{ex}(k)) - f(E_{cb}(k))] \delta(E_{ex}(k) - E_{cb}(k) - E) \quad (S1)$$

With E_{ex} and E_{cb} is the energy of the exciton and continuum band (CB or VB), respectively; $f(E)$ is the Fermi-Dirac distribution function, and M is the matrix element for the transition.

The exciton wave function is localized in real space over a distance, l and thus the exciton is not a δ -function in k -space; but instead is spread over a range, Δk in k , where $\Delta k \approx 1/l$. Therefore we have to integrate over $k < \Delta k$

$$\alpha(E) \propto \frac{1}{E} \int d^2q |M(q)|^2 |C(q)|^2 \delta(E_{ex}(q) - E_{cb}(q) - E), \quad (S2)$$

Where $C(q)$ is a ‘mixture function’ that is spread over Δk , and determines the k -space extension of the exciton wavefunction. We replace the Fermi-Dirac distribution function with a step function at E_B , if the exciton temperature is low compared to exciton binding energy, E_B .

If we assume that the exciton wave function in real space has the form of $\propto \exp(-r/l)$, where l is the ‘localization length’, then $C(q)$ is given by the Fourier transform of the real space extension,

$$C(q) \propto (1 + l^2 q^2)^{-1} \quad (S3)$$

Consequently the k -space exciton extension, $\Delta k = l^{-1}$, and the absorption, $\alpha(E)$ for a 2D system can be then expressed by [S4]:

$$\alpha(E) \propto \frac{(E - \Delta_0)}{E} \left(\frac{1}{E - \Delta_0 + \hbar^2 / 2l^2 m^*} \right)^2 \quad (S4)$$

where m^* is the electron effective mass, and Δ_0 is the transition energy. We calculated the exciton PA using $m^* = 0.25 m_0$, where m_0 is the free electron mass [S5], and $\Delta_0 = 0.35$ eV. The asymmetric PA₁ band is fitted using Eq. (S4) considering a Gaussian distribution $F(\Delta - \Delta_0)$ of Δ around Δ_0 (see Fig. 3A) having width $\delta\Delta$. From the fit we get the exciton localization length, $l = 10$ nm, $\Delta_0 = 0.35$ eV, and the distribution width $\delta\Delta = 0.05$ eV.

Inter-Rashba optical transitions in 2D perovskites

To illustrate the essential features of the electronic structure and optical response of the system, we present an effective tight-binding model for the conduction and valence bands of the 2D perovskite. As in the 3D perovskite $\text{CH}_3\text{NH}_3\text{PbI}_3$ [S6], the conduction band is derived from Pb p -orbitals. Due to the high spin-orbit of the heavy Pb atom, the $J = 1/2$ split off band is well separated in energy from the $J = 3/2$ bands, and forms the basis for the conduction band states. In terms of orbitals $p_{x,y,z}$ and spin \uparrow, \downarrow , the $|J_{\pm 1/2}\rangle$ states are:

$$\begin{aligned} |J_{+1/2}\rangle &= \frac{-1}{\sqrt{3}}(|p_x, \downarrow\rangle + i|p_y, \downarrow\rangle + |p_z, \uparrow\rangle) \\ |J_{-1/2}\rangle &= \frac{-1}{\sqrt{3}}(|p_x, \downarrow\rangle - i|p_y, \downarrow\rangle - |p_z, \uparrow\rangle) \end{aligned} \quad (\text{S5})$$

The valence band is comprised of Pb and I orbitals with $s = 1$ symmetry:

$$\begin{aligned} |S_{+1/2}\rangle &= |s, \uparrow\rangle \\ |S_{-1/2}\rangle &= |s, \downarrow\rangle \end{aligned} \quad (\text{S6})$$

It suffices to consider a square 2D lattice. The ss , pp , and sp hopping terms are denoted t_{ss} , t_{pp} , and ξ , respectively. Breaking inversion symmetry introduces additional spin-dependent hopping terms. For structural inversion symmetry breaking along the x -direction, spin-orbit coupling leads to a k_y -dependent effective magnetic field in the z -direction acting on the $J = \pm 1/2$ states. We parameterize this Rashba spin-orbit coupling with a constant γ . The symmetry breaking also leads to additional terms coupling s and p states, which we parameterize with γ' . The tight-binding Hamiltonian then takes the following form (where the basis ordering is: $|S_{+1/2}\rangle, |S_{-1/2}\rangle, |J_{+1/2}\rangle, |J_{-1/2}\rangle$):

$$H = \begin{pmatrix} -t_{ss}k^2 & 0 & 0 & \xi(ik_- + \gamma') \\ 0 & -t_{ss}k^2 & \xi(-ik_+ + \gamma') & 0 \\ 0 & \xi(ik_- + \gamma') & t_{pp}k^2 + \gamma k_y + \epsilon_0 & 0 \\ \xi(-ik_+ + \gamma') & 0 & 0 & t_{pp}k^2 - \gamma k_y + \epsilon_0 \end{pmatrix}, \quad (\text{S7})$$

where $k_{\pm} = k_x \pm ik_y$, $k^2 = k_x^2 + k_y^2$. k is dimensionless, scaled by the lattice constant a , and we assume $ka \ll 1$. The constant ϵ_0 determines the band gap. To make analytical progress, we consider a perturbation expansion in ξ/ϵ_0 . (Note that in Eq. (S7) we rescaled the inversion asymmetry sp hopping parameter γ' to $\xi\gamma'$ so that we can do an expansion of the conduction-valence coupling in terms of the single parameter ξ .) Assuming $k_x = 0$, the (unnormalized) conduction band wave functions to lowest order in ξ are:

$$\begin{aligned} \psi_{c1} &= |J_{+1/2}\rangle + \left(\frac{\xi(ik_y + \gamma')}{ik_y^2 - \gamma k_y + \epsilon_0} \right) |S_{-1/2}\rangle, \\ \psi_{c2} &= |J_{-1/2}\rangle + \left(\frac{\xi(-ik_y + \gamma')}{ik_y^2 - \gamma k_y + \epsilon_0} \right) |S_{+1/2}\rangle \end{aligned} \quad (\text{S8})$$

Where $\mathbf{t} = \mathbf{t}_{ss} + \mathbf{t}_{pp}$. The lowest order contribution to the conduction and valence band energies enters as ξ^2 :

$$E_c = (t_{pp}k_y^2 \pm \gamma|k_y| + \epsilon_0) + \frac{\xi^2(\gamma'^2 + k^2)}{tk_y^2 \pm \gamma k_y + \epsilon_0} \quad (\text{S9})$$

$$E_v = -t_{ss}k_y^2 + \frac{\xi^2(\gamma'^2 + k^2)}{tk_y^2 \pm \gamma k_y + \epsilon_0} \quad (\text{S10})$$

Note that the valence band degeneracy is lifted through the hybridization with the conduction band. The minimum of the conduction k_0 is found using Eq. (S9), and given here to lowest order in ξ :

$$k_0 = \frac{\gamma}{2t_{pp}} + \frac{\xi^2 2\gamma t_{pp}(\gamma'^2 + 4t_{ss}t_{pp}\gamma'^2 - 4t_{pp}\epsilon_0)}{(t_{ss}\gamma'^2 - t_{pp}\gamma'^2 + 4t_{pp}^2\epsilon_0)^2} \quad (\text{S11})$$

We may now compute the dipole matrix element between conduction band states at k_0 . We find that only the z -component is nonzero:

$$\langle \psi_{c1} | z | \psi_{c2} \rangle = 2t_{pp}\xi d_{sp}^z \left(\frac{t\gamma + 2it_{pp}\gamma'}{t_{ss}\gamma'^2 - t_{pp}\gamma'^2 + 4t_{pp}^2\epsilon_0} + \frac{t\gamma - 2it_{pp}\gamma'}{t_{ss}\gamma'^2 + 3t_{pp}\gamma'^2 + 4t_{pp}^2\epsilon_0} \right) \quad (\text{S12})$$

Where $d_{sp}^z = \langle s | z | p_z \rangle$. Although the expression above is cumbersome, the significant result is simply that it is nonzero. This can also be understood by inspecting the form of the wave functions given in Eq. (S8). The sp hybridization present in ψ_{c1} and ψ_{c2} enable an optical transition between the two. We note that the incident light is mostly polarized in the xy plane, however the light is incoherent and diffuse, as described earlier in the S.I., so that a z -component of the polarization is also generically present.

Density Functional Theory calculations

We carry out first-principles density functional theory (DFT) calculations using local density approximation in the form of ultra-soft pseudopotentials as implemented in QUANTUM-ESPRESSO. An energy cutoff of 80 Ry and a $6 \times 6 \times 1$ grid was employed for the plane wave basis expansion and for the Brillouin zone sampling during structural relaxation, respectively. All atoms in the unit cell were allowed to move until the force on each is less than 0.5 eV/nm. The lattice parameters are calculated to be $a = 0.619$ nm, $b = 0.623$ nm, $c = 3.025$ nm and 99.67° for the angle between lattice vectors \mathbf{a} and \mathbf{b} , in good agreement with the experimental measurements ($a = 0.613$ nm, $b = 0.619$, $c = 3.251$ nm and 93.80° (S7)). Similar to the three-dimensional halide perovskites, the near-gap energy states in $(\text{C}_6\text{H}_5\text{C}_2\text{H}_2\text{NH}_3)_2\text{PbI}_4$ are dominated by the orbitals in the two-dimensional inorganic framework and therefore, we are concerned with the symmetry properties of the inorganic framework. As shown in Figure 4A, inversion symmetry is present in the z -direction, normal to the two-dimensional inorganic framework. The displacement of the Pb atom off the octahedral center leads to inversion symmetry breaking in the x - y plane. The symmetry breaking direction is roughly along the $\mathbf{a} + \mathbf{b}$ direction.

The electronic structure exhibits a direct band gap at the R point in the BZ $[2\pi/a, 2\pi/b, 0]$, where a and b are the lattice constants. The near-gap conduction band states are composed of the p orbitals of Pb while the valence bands states are derived from the Pb s orbital and $I p$ orbitals. The spin-orbit coupling splits degenerate conduction band states ($L = 1$) into lower $J = 1/2$ and upper $J = 3/2$ bands, leading to a $J = 1/2$ conduction band and $S = 1/2$ valence band. In order to observe symmetry breaking effect on the band structure, bands along two paths are plotted as shown in Figure 4C. One is aligned with symmetry breaking direction from $X=(0.0, 0.0, 0.0)$ to $R=(0.5, 0.5, 0.0)$ and the other is along the normal direction from $R=(0.5, 0.5, 0.0)$ to $Y=(0.0, 1.0, 0.0)$. The band along X-R is nearly degenerate, whereas bands along R-Y exhibit Rashba-like splitting.

We now consider the photogenerated free carrier absorption, i.e., the transition between Rashba-split conduction bands. Using DFT, we calculated the momentum matrix element between Rashba-split bands. We use a plane wave basis and the Bloch wave function is described as $|\Psi_{n\mathbf{k}}\rangle = \frac{1}{V} \sum_{\mathbf{G}} c_n(\mathbf{k} + \mathbf{G}) e^{i(\mathbf{k} + \mathbf{G}) \cdot \mathbf{r}}$, where V is the crystal volume, \mathbf{G} is the reciprocal lattice vector, \mathbf{k} is the crystal momentum and $c_n(\mathbf{k} + \mathbf{G})$ is the coefficient of plane wave $e^{i(\mathbf{k} + \mathbf{G}) \cdot \mathbf{r}}$. The momentum matrix element was calculated as $\langle \Psi_{m\mathbf{k}} | \hat{p}_\alpha | \Psi_{n\mathbf{k}} \rangle = \hbar \sum_{\mathbf{G}} c_m^*(\mathbf{k} + \mathbf{G}) c_n(\mathbf{k} + \mathbf{G}) (\mathbf{k} + \mathbf{G})_\alpha$, where α refers to the momentum direction x, y or z . In Figure 4D we show the dipole transition magnitude as a function of k along the direction with largest splitting that is also the direction normal to the inversion symmetry breaking. As seen, *the optical transition between the two Rashba-split CB is allowed*, in agreement with the tight-binding model described above.

Fitting the PA_{FCA} band shown in Fig. 5A

A slight asymmetry is also observed for PA_{FCA} band in Fig. 5A, which suggests that the electron quasi momentum k near the bottom of the lower Rashba-split band at k_0 may also extend in k -space. This may be due to localization or the quasi-Fermi level of electrons in this band. Using Eq. S4, we fit the PA_{FCA} band (solid line in Fig. 5A), using the same model as that for the exciton transition in Fig. 3A inset. We used the same Gaussian distribution for the transition energy with $\Delta_0 = 0.15$ eV and $\delta\Delta = 0.03$ eV, as for the exciton PA model described above. The “localization length” or “wavefunction extent” of the electron that we obtained from the fit is ~ 14 nm. This shows that the electron is barely localized, consistent with of the free-electron model of electron in conduction band.

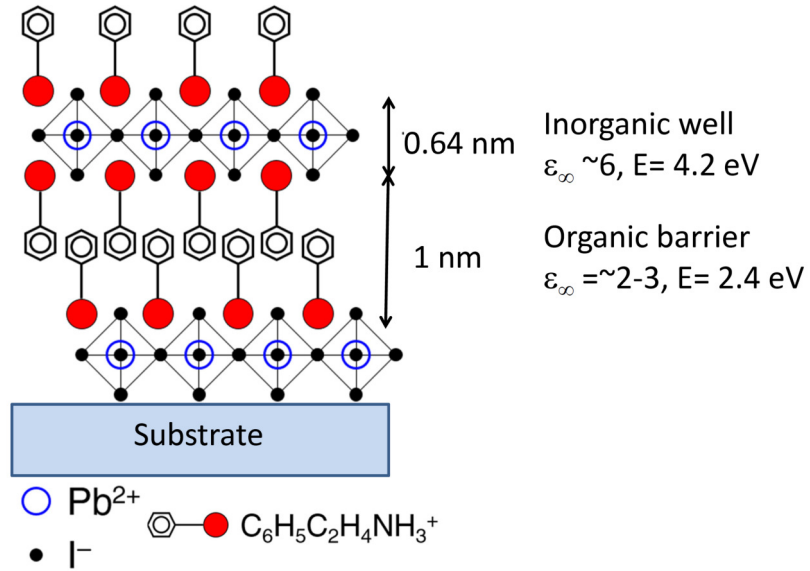


Fig. S1.

Schematic structure of $(\text{C}_6\text{H}_5\text{C}_2\text{H}_4\text{NH}_3)_2\text{PbI}_4$ (PEPI) with alternating organic and inorganic layers, forming multiple quantum well onto the substrate. The width, energy gap, dielectric constant of barriers, and well are denoted [S1, S2].

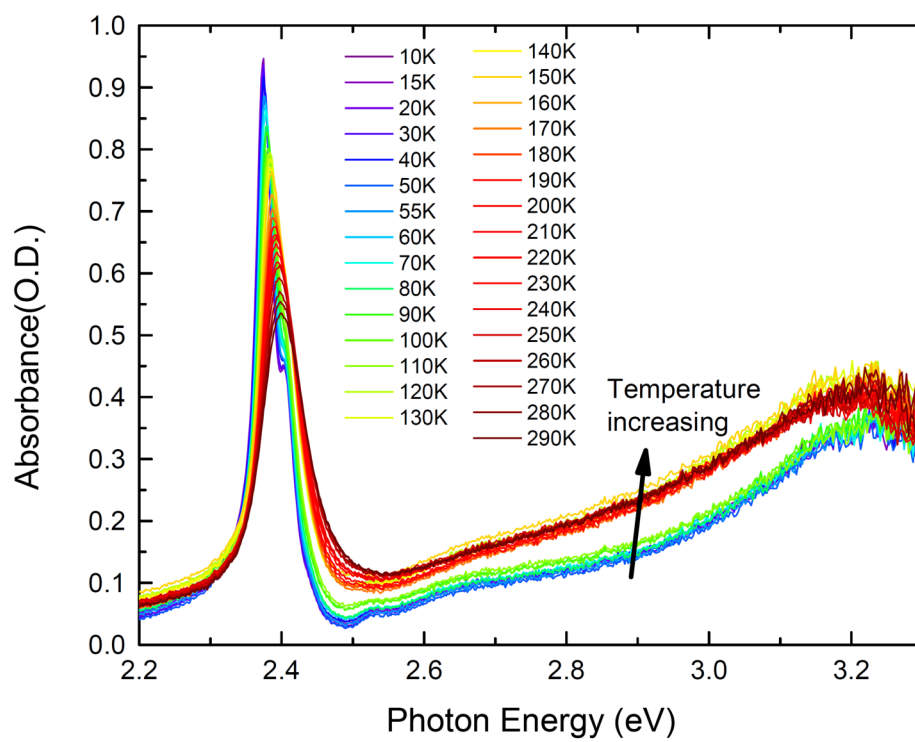


Fig. S2

The absorption spectrum of a PEPI film measured at temperatures ranging from 10K to 290K as denoted.

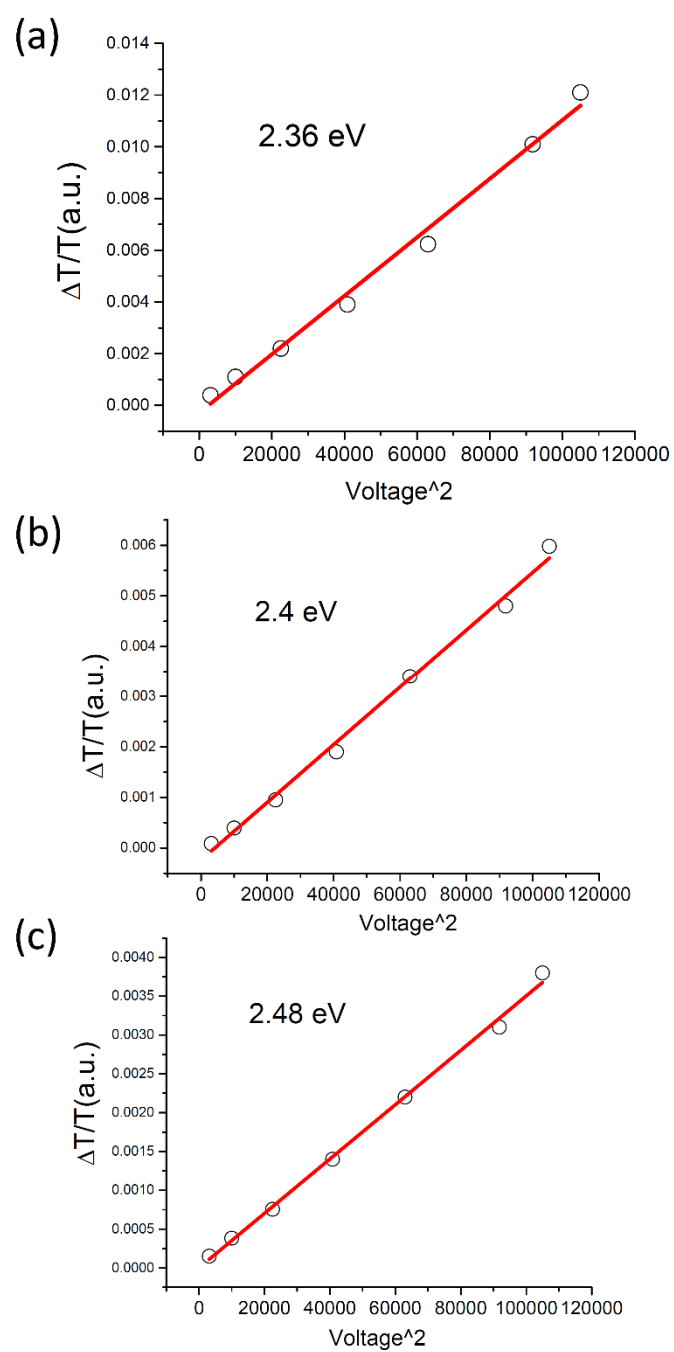


Fig. S3

The dependence of the EA signal on V^2 at various energies below the IB-edge at 2.55 eV, where V is the applied voltage.

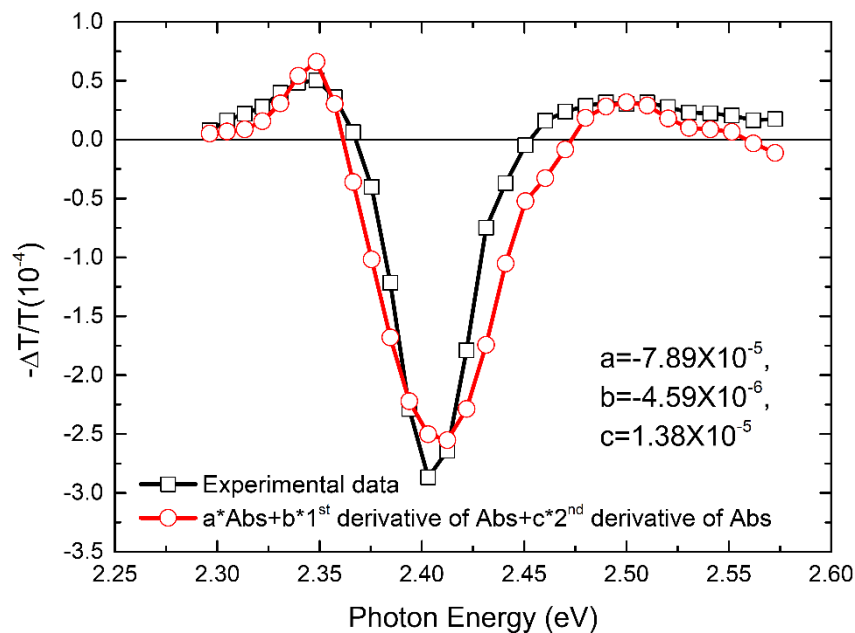


Fig. S4

The transient PM band of PEPI film measured at $t=0$ ps and 300K, and its fit using a linear combination of the absorption spectrum and its first and second derivatives.

References and notes:

- [S1] T. Ishihara, J. Takahashi, and T. Goto, *Optical properties due to electronic transitions in two-dimensional semiconductors $(C_nH_{2n+1}NH_3)_2PbI_4$* , Phys. Rev. B **42**, 11099 (1990),
- [S2] X. Hong, T. Ishihara, and A. U. Nurmikko, *Dielectric confinement effect on excitons in PbI_4 -based layered semiconductors*, Phys. Rev. B **45**, 6961(1992)
- [S3] G. Bastard, *Wave mechanics applied to semiconductor heterostructures* (Les Edition de Physique, Les Ulis, France, 1988)
- [S4] M. Olszakier, E. Ehrenfreund, and E. Cohen, *Determination of the extension of the heavy hole wave function in GaAs by photomodulation spectroscopy* Phys. Rev. B **43**, 9350 (1991)
- [S5] Z. Guo, X. Wu, T. Zhu, X. Zhu, and L. Huang, *Electron-phonon scattering in Atomically Thin 2D perovskite* ACS Nano **10**, 9992 (2016)
- [S6] J. Even, L. Pedesseau, J.-M. Jancu, and C. Katan, *Importance of Spin-Orbit Coupling in Hybrid Organic/Inorganic Perovskites for Photovoltaic Applications* J. Phys. Chem. Lett **4**, 2999 (2013).
- [S7] [J. Am. Chem. Soc. 113, 2328 (1991)].